Dalton Transactions

PAPER

View Article Online
View Journal | View Issue

Cite this: *Dalton Trans.*, 2014, **43**, 3162

Ln[DO3A-*N*-α-(pyrenebutanamido)propionate] complexes: optimized relaxivity and NIR optical properties†

M. F. Ferreira,[a] G. Pereira,[a] A. F. Martins,[b,c] C. I. O. Martins,[b] M. I. M. Prata,[d] S. Petoud,[c] E. Toth,[c] P. M. T. Ferreira,[a] J. A. Martins*‡[a] and C. F. G. C. Geraldes[b]

Received 21st October 2013,
Accepted 20th November 2013

DOI: 10.1039/c3dt52958d

www.rsc.org/dalton

We have proposed recently that the DO3A-*N*-α-(amino)propionate chelator and its amide conjugates are leads to targeted, high relaxivity, safe contrast agents for magnetic resonance imaging. In this work we illustrate further the expeditious nature and robustness of the synthetic methodologies developed by preparing the DO3A-*N*-(α-pyrenebutanamido)propionate chelator. Its Gd^{3+} chelate retains the optimized water exchange, high stability and inertness of the parent complex. The pyrene moiety imparts concentration-dependent self-assembly properties and aggregation-sensitive fluorescence emission to the Gd^{3+} complex. The Gd^{3+} complex displays pyrene-centred fluorescence whilst the Yb^{3+} and Nd^{3+} complexes exhibit sensitized lanthanide-centred near-infrared luminescence. The aggregated form of the complex displays high relaxivity (32 mM^{-1} s^{-1}, 20 MHz, 25 °C) thanks to simultaneous optimization of the rotational correlation time and of the water exchange rate. The relaxivity is however still limited by chelate flexibility. This report demonstrates that the DO3A-*N*-(α-amino)propionate chelator is a valuable platform for constructing high relaxivity CA using simple design principles and robust chemistries accessible to most chemistry labs.

Introduction

Positron emission tomography (PET), single photon emission correlated tomography (SPECT), magnetic resonance imaging (MRI), ultra sound (US), and X-ray computerized axial tomography (CAT) are imaging modalities used nowadays regularly in hospitals for diagnostic and prognostic purposes.[1] MRI has become in recent years the most useful imaging modality in the clinical setup. This results from its superb spatial resolution, use of non-ionizing radiation (radiofrequencies and magnetic fields), depth independent imaging and the possibility of repeated imaging to offset the low detection sensitivity of MRI which is intrinsic to the nuclear magnetic resonance phenomenon. Signal intensity differences in MRI (contrast) arise mainly from intrinsic differences of the relaxation times ($T_{1,2}$) of the water protons of tissues. The contrast between normal and diseased tissues can be dramatically improved by paramagnetic contrast agents (CA) (Gd^{3+}, Mn^{2+}, stable nitroxide radicals, iron oxide nanoparticles, *etc.*), which shorten the relaxation times of the water protons.[2] Relaxivity ($r_{1,2}$), which is the paramagnetic enhancement of water proton relaxation rates $R_{1,2}$ ($R_{1,2} = 1/T_{1,2}$) normalized to 1 mM concentration, measures CA efficacy.[2,3] The currently used CAs for T_1-weighted MRI imaging are Gd^{3+} chelates of linear (DTPA-type) or macrocyclic (DOTA-type) poly(aminocarboxylate) chelators.

[a]*Centro de Química, Campus de Gualtar, Universidade do Minho, 4710-057 Braga, Portugal. E-mail: jmartins@quimica.uminho.pt, jarm20@bath.ac.uk*
[b]*Department of Life Sciences, Faculty of Science and Technology, Centre of Neurosciences and Cell Biology, and Coimbra Chemistry Centre, University of Coimbra, 3001-401 Coimbra, Portugal*
[c]*Centre de Biophysique Moléculaire CNRS, Rue Charles Sadron, 45071 Orléans Cedex 2, France*
[d]*ICNAS and IBILI, Faculty of Medicine, University of Coimbra, 3000-548 Coimbra, Portugal*

† Electronic supplementary information (ESI) available: Size distribution in: (a) volume (%); (b) intensity (%) for a Gd**L** solution (5 mM, pH 7.0, 25 °C) at a concentration well above the cmc (0.6 mM) (Fig. S1); temperature dependence of the water proton relaxivity for Gd**L** (20 MHz, 1 mM, pH 6.0) (Fig. S2); pH dependence of the water proton relaxivity for Gd**L** (20 MHz, 1 mM, 25 °C) (Fig. S3); time evolution of $R_{1p}(t)/R_{1p}(0)$ (20 MHz, pH 7.1, 25 °C) for a 1.5 mM solution of Gd**L** in 10 mM phosphate buffer without and with an equimolar amount of Zn^{2+} (Fig. S4); UV-Vis spectra for the free ligand **L** and the Gd**L** complex (Fig. S5); fluorescence spectra for the free ligand **L** in non-deoxygenated water (pH 7.0) over the concentration range 5×10^{-5}–5×10^{-3} mol dm^{-3} (λ_{exc} = 345 nm) (Fig. S6); changes in ratio excimer/monomer emission (I_E/I_M) for ligand **L** as a function of the ligand concentration (Fig. S7); best fit values for the fitting of the experimental data of I_{Exc}/I_{Mono} *vs.* [GdL] (Table S1); biodistribution of ^{153}Sm**L** in Wistar rats 1 and 24 hours after i.v. injection (Table S2); equations for the analysis of ^{1}H NMRD and ^{17}O NMR data (Appendix 1). See DOI: 10.1039/c3dt52958d

‡ Currently on sabbatical leave at the Dep. Chemistry University of Bath, UK.

Due to its long electronic relaxation times and high paramagnetism, Gd^{3+} efficiently enhances T_1 relaxation, resulting in signal intensity enhancement and bright images – positive contrast.[4] High relaxivity CA can lead to T_1 reductions sufficient to generate effective contrast at low doses. Moreover, delivering CA to diseased areas can allow further dose reduction. Effective contrast at low CA doses (CAs in clinical use are normally used at a dose of 0.1 mmol kg^{-1}) became more important recently with the identification of the nephrogenic systemic fibrosis (NSF) which is a debilitating and even deadly condition associated with *in vivo* Gd^{3+} release from Gd-based CAs.[5] In fact, free (non-complexed) Gd^{3+} (and all the other Ln^{3+} ions) are acutely toxic. Most NSF cases have been associated with the use of Gd^{3+} DTPA-type complexes, particularly Gd(DTPA-bis-amide) CA.[6] Low thermodynamic stability and kinetic lability, coupled to slow kidney clearance, results in extensive complex demetallation *in vivo*.[7] Macrocyclic, DOTA-type Gd^{3+} complexes are generally considered safe given their higher thermodynamic stability and kinetic inertness.[8] Chelates displaying simultaneous optimization of the molecular parameters that govern relaxivity, namely the rotational correlation time (τ_R), the water exchange rate ($k_{ex} = 1/\tau_M$) and the electronic relaxation parameters, are expected to display very high relaxivities.[9] There are well established strategies for tuning τ_R and k_{ex} into the optimal range to attain high relaxivities at intermediate fields relevant for clinical MRI. Tuning the Gd^{3+} ion electronic relaxation parameters turns out to be more challenging.[10] Increasing the molecular weight of chelates leads to longer rotational correlation times (τ_R) (slower tumbling rates) enhancing CA relaxivity at intermediate fields.

Self-assembly of amphiphilic chelates into micelle-type supramolecular structures,[11] non-covalent association with serum albumin[12] and covalent attachment of chelates to macromolecular and nanoobjects (proteins,[13] dendrimers,[14] nanoparticles,[15] viral capsules,[16] quantum dots,[17] *etc.*) are well established strategies to tune τ_R. Replacement of an ethylenediamine by a propylenediamine bridge or a pendant acetate by a propionate group on the DOTA and DTPA scaffolds enforces steric compression around the water binding site on Gd^{3+} complexes, leading to accelerated water exchange.[11,18,19] A pendant propionate group leads to water exchange rate enhancements suitable for attaining high relaxivities at intermediate fields, without compromising the thermodynamic and kinetic stability of the chelates.[18,20,21] Still, connecting linkers/spacers permit fast local rotational motions of the immobilized chelates superimposed on global slow rotational motions of the (entire) macromolecular object, resulting in suboptimal effective rotational correlation times.[11,15]

Endowing targeted high relaxivity Gd^{3+} chelates with a fluorescence reporting capability results in bimodal MRI/fluorescence imaging agents. This approach has the potential to improve CA performance: the high detection sensitivity of fluorescence complements the low detection sensitivity of MRI, whilst the depth independent properties of MRI complement the limited light crossing into live tissues.[22]

Conjugates of metal chelate-fluorophores,[23] quantum dots,[17,24] silica nanoparticles[25,26] and other nanomaterials functionalised with Gd^{3+} chelates have been described as bimodal MRI/fluorescence imaging agents. The aggregation sensitive fluorescence properties of the pyrene fluorophore[27] make pyrene conjugates especially attractive as "responsive" probes for structural,[28] biochemical and cellular studies[29] and as chemical sensors.[30] Moreover, pyrene has been used as an antenna for sensitizing near infrared (NIR) emitting Ln^{3+} ions (Yb^{3+}, Nd^{3+} and Er^{3+}) in DOTA and DTPA chelates.[31,32]

We have recently described methodologies for the synthesis of the DO3A-*N*-(α-amino)propionate chelator and for preparing its amide conjugates.[18,21] Gd^{3+} complexes of those amide conjugates retain the optimal water exchange, high stability and kinetic inertness of the parent complex.[18] In this work we describe the synthesis of the pyrenebutyric acid conjugate of the DO3A-*N*-(α-amino)propionate chelator and its Ln^{3+} complexes. The effect of self-assembly on the relaxivity and fluorescence properties of the Gd[(DO3A-*N*-(α-pyrenebutanamido)-propionate)] complex was studied by relaxometry and steady state fluorescence. The potential of the pyrene moiety to sensitize NIR emitting Ln^{3+} ions has also been addressed.

Results and discussion

Synthesis

The DO3A-*N*-(α-pyrenebutanamido)propionate chelator (**L**) was synthesised following the (indirect) methodology proposed before for amide conjugates of the DO3A-*N*-(α-amino)propionate chelator (Scheme 1).[21]

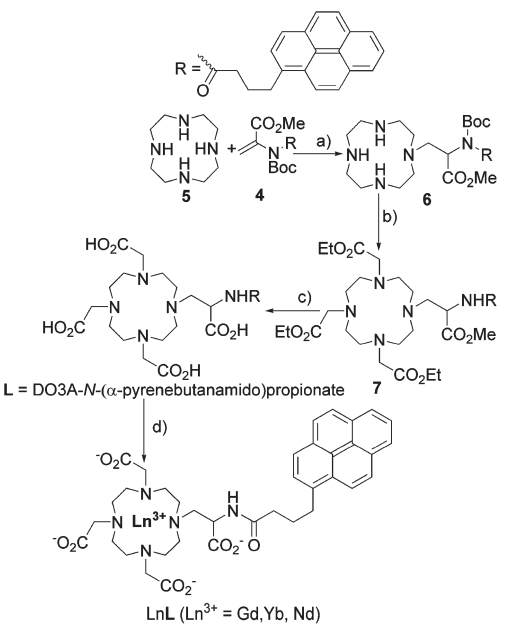

Scheme 1 Synthetic pathway for the metal chelator DO3A-*N*-(α-pyrenebutanamido)propionate (**L**) and its Ln^{3+} complexes LnL: (a) K_2CO_3/MeCN; (b) i. TFA/DCM, ii. ethyl bromoacetate, K_2CO_3/MeCN; (c) i. Dowex 1X2-OH^-, ii. elution with hydrochloric acid 0.1 M; (d) $LnCl_3 \cdot xH_2O$.

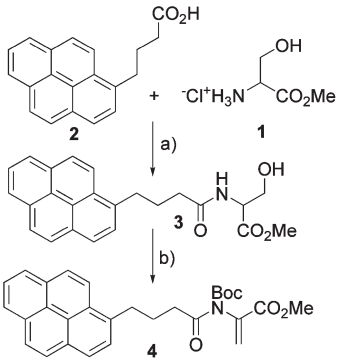

Scheme 2 Synthesis of the dehydroalanine (Pyrene, Boc)-Δ-AlaOMe reactive block (**4**): (a) i. TEA 2 molar equivalents/MeCN, ii. DCC/HOBt; (b) Boc_2O, DMAP, dry MeCN.

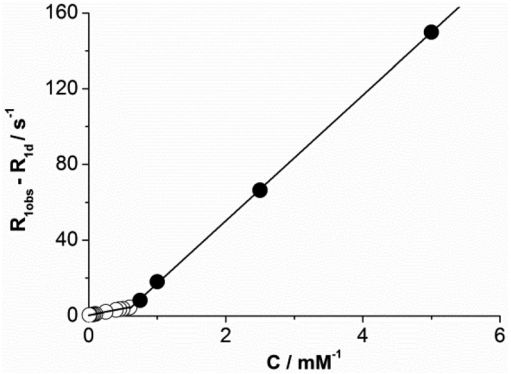

Fig. 1 Concentration dependence of the paramagnetic water proton longitudinal relaxation rate R_{1p} = (R_1^{obs} – R_1^{d}) for GdL (20 MHz, 25 °C, pH 7.0).

The *N*-(α-pyrenebutanamido)propionate pendant group was introduced, early on the synthesis, into the *cyclen* scaffold *via* Michael addition of the dehydroalanine (Pyrene, Boc)-Δ-AlaOMe reactive block (**4**). Synthetic block (**4**) was prepared in 2 steps in 70% overall yield following the procedure developed by Ferreira and co-workers (Scheme 2).[33]

After removing the *tert*-butyloxycarbonyl protecting group from the monoalkylated intermediate (**6**) with TFA, one pot N-alkylation of the *cyclen* scaffold with ethyl bromoacetate afforded prochelator **7**. Alkaline deprotection of **7** with Dowex 1X2-OH^- resin, followed by resin elution with diluted hydrochloric acid, afforded the DO3A-*N*-(α-pyrenebutanamido)-propionate chelator (**L**) as hydrochloride in 30% overall yield over 3 steps. Recently, Caravan and co-workers have reported a similar pathway for the synthesis of conjugates of the DO3A-*N*-(α-amino)propionate chelator.[34] The synthesis of the DO3A-*N*-(α-pyrenebutanamido)propionate chelator further supports the use of the *indirect* pathway for amide conjugates of the DO3A-*N*-(α-amino)propionate chelator.

Relaxometric studies of the GdL complex

The concentration dependence of the paramagnetic water proton relaxation rate (R_{1p}) was evaluated for Gd**L** (20 MHz, 25 °C, pH 7.0) in the concentration range 0.05–5.0 mM (Fig. 1).

The paramagnetic longitudinal relaxation rate data *vs.* [Gd**L**] define two straight lines with different slopes. This behaviour is characteristic of chelate self-assembly in aqueous solution, presumably into micelle-type structures, driven by the hydrophobic effect.[11] The break point gives an estimation of the critical micelle concentration, cmc (0.60 ± 0.02 mM), for Gd**L**. Below the cmc, the complex is in a monomeric, non-aggregated form in solution (eqn (1)). Above the cmc, it is present in the form of aggregates as well as monomers whose concentration corresponds to the cmc (eqn (2)). R_1^d is the diamagnetic contribution to the longitudinal relaxation rate (the relaxation rate of pure water), $r_1^{n.a}$ (6.86 ± 0.03 mM^{-1} s^{-1}) represents the relaxivity of the free, non-aggregated Gd^{3+} chelate, r_1^a (33.11 ± 0.04 mM^{-1} s^{-1}) is the relaxivity of the micellar (aggregated) form and C_{Gd} is the analytical Gd^{3+} concentration.

$$R_{1p} = R_1^{obs} - R_1^{d} = r_1^{n.a} \times C_{Gd} \quad (1)$$

$$R_{1p} = R_1^{obs} - R_1^{d} = (r_1^{n.a} - r_1^{a}) \times cmc + r_1^{a} \times C_{Gd} \quad (2)$$

The micellar nature of Gd**L** above the cmc (5.0 mM, pH 7.0) was confirmed by dynamic light scattering (DLS) analysis (Fig. S1†). A bimodal intensity distribution, with the main population of particles displaying an average radius of 1.7 nm and a minor population exhibiting an average radius of 73 nm, was obtained by DLS, resulting in a population weighted mean hydrodynamic radius, expressed by the *z*-average parameter, of 49 nm. The temperature (Fig. S2†) and pH dependences (Fig. S3†) of the paramagnetic water proton relaxation rate were studied at 20 MHz. Transmetallation studies against Zn^{2+} ions were also performed to evaluate the kinetic inertness of the complex (Fig. S4†). The temperature dependence study strongly suggests that below 50 °C, the relaxivity is not limited by slow water exchange. The pH-dependence and the transmetallation studies indicate that the Gd**L** complex, like its non-associating Gd[(DO3A-*N*-(α-benzoylamido)propionate)] analogue, is stable towards protonation-assisted demetallation and inert towards transmetallation with Zn^{2+}.[21]

^{17}O NMR and ^{1}H NMRD studies

The magnetic field dependence of the longitudinal water proton relaxivities (^1H NMRD profiles) of Gd**L** was recorded at 25 °C and 37 °C in the frequency range 0.01 to 80 MHz and at concentrations below (Fig. 3) and above (Fig. 2c) the cmc. The NMRD curves are influenced by many parameters, the most important being the hydration number (q), the water exchange rate (k_{ex}), the electron relaxation parameters (τ_v and Δ^2) and the rotational correlation time (τ_R). The NMRD measurements have been completed with ^{17}O NMR data (Fig. 2a and b). Indeed, from variable temperature ^{17}O T_2 measurements, one can accurately determine the water exchange rate. The rotational correlation time can be assessed by variable temperature ^{17}O T_1 measurements. On the other hand, variable

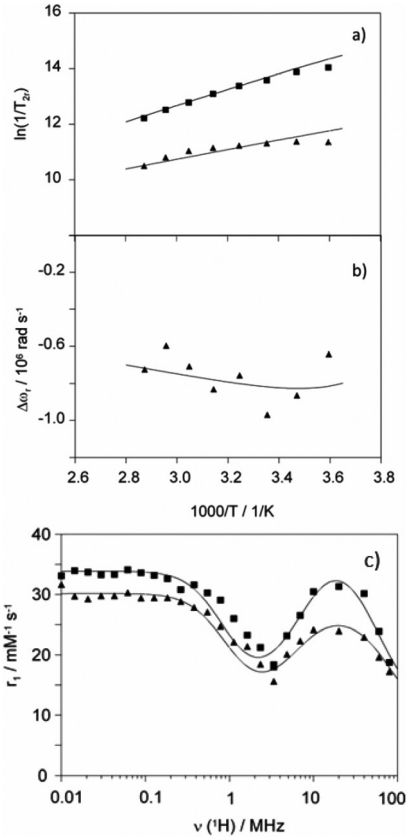

Fig. 2 Temperature dependence of (a) reduced longitudinal, T_{1r} (■), and transverse, T_{2r} (▲), relaxation times and (b) chemical shifts ($\Delta\omega_r$) of a micellar aqueous solution of Gd**L** at 11.7 T (5.0 mM, pH 7.0); (c) NMRD profiles of the aggregated micellar state (2.5 mM, pH 7.0) at 25 °C (■) and 37 °C (▲) after subtraction of the relaxation contribution of the monomer form. The curves represent results from the simultaneous fittings as described in the text.

temperature measurements of the chemical shift difference between bulk and bound water ($\Delta\omega_r$) give an indication of the q value.

The proton relaxation rates measured above the cmc represent the sum of the relaxivity contribution of the monomer complex, present at a concentration equal to the cmc, and the relaxivity contribution of the aggregated state. In order to calculate the relaxivity of the aggregated form, the relaxivity contribution of the monomer has been subtracted from the relaxation rates measured above the cmc. These profiles present the characteristic high field peak typical of slowly tumbling Gd^{3+} complexes. The ^{17}O NMR measurements have been performed at 5.0 mM concentration, largely above the cmc (0.6 mM). Under these conditions, one can consider that the rotational dynamics, as assessed by ^{17}O T_1 data, corresponds to the micellar state. Therefore, the ^{17}O NMR data have been fitted together with the NMRD curves of the micellar state to the Solomon–Bloembergen–Morgan theory by including the Lipari–Szabo treatment for the description of the rotational motion (Table 1).[35] In this approach, two kinds of motion are assumed to modulate the interaction causing the relaxation,

Table 1 Best fit parameters obtained for the aggregated form of Gd**L** from the simultaneous analysis of the ^{17}O NMR and ^{1}H NMRD data and for the monomer from NMRD data[a]

Parameter	Aggregated form	Monomer
$\Delta H^{\ddagger}$ [kJ mol^{-1}]	21.5 ± 1.5	*21.5*
k_{ex}^{298} [10^7 s^{-1}]	6.2 ± 0.5	*6.2*
τ_g^{298} [ps]	3780 ± 100	116 ± 5
τ_{lO}^{298} [ps]	930 ± 50	—
S^2	0.24 ± 0.02	—
$\tau_{lH}^{298}/\tau_{lO}^{298}$	0.80 ± 0.05	—
E_g [kJ mol^{-1}]	25.4 ± 0.7	—
E_l [kJ mol^{-1}]	12 ± 1	24.3 ± 0.2
Δ^2 [10^{20} s^{-1}]	0.033 ± 0.004	0.38 ± 0.04
τ_v^{298} [ps]	53 ± 5	6.3 ± 0.5
$A/\hbar$ [10^6 rad s^{-1}]	−3.2 ± 0.4	—

[a] Parameters in italics have been fixed; τ_{RO}^{298} values from ^{17}O T_1 data.

namely a rapid, local motion which lies in the extreme narrowing limit and a slower, global motion.

We calculate therefore τ_g, the correlation time for the global motion (common to the whole micelle), and τ_l, the correlation time for the fast local motion, which is specific for the individual relaxation axis and thus related to the motion of the individual Gd^{3+} chelate units. The generalized order parameter, S, is a model-independent measure of the degree of spatial restriction of the local motion, with $S = 0$ if the internal motion is isotropic and $S = 1$ if the motion is completely restricted.

It was assumed that the Gd**L** complex has one inner sphere water molecule ($q = 1$) like the low molecular weight amide analogue Gd[(DO_3A-*N*-(α-benzoylamido)propionate)][21] and the parent amine Gd[(DO_3A-*N*-(α-amino)propionate)].[18] This assumption was confirmed by the value obtained for the scalar coupling parameter ($A/\hbar = -3.2 \times 10^6$ rad s^{-1}).[36]

The NMRD curves of the monomer sample (0.3 mM) have been analyzed by fixing the water exchange parameters (k_{ex}^{298}, $\Delta H^{\ddagger}$) to those obtained from the ^{17}O NMR data. In the fits, we have fixed the r_{GdH} distance to 3.10 Å and the distance of closest approach of the bulk water protons to the Gd^{3+}, a_{GdH}, to 3.65 Å. The diffusion constant has been fixed to 23×10^{-10} m^2 s^{-1} and its activation energy to 20 kJ mol^{-1}.

The NMRD profile for the monomeric form is characteristic of low molecular weight complexes (Fig. 3). The relaxivity at intermediate field (5.9 mM^{-1} s^{-1}; 25 °C, 20 MHz) is dominated by fast rotation in solution as indicated by the short τ_R value obtained (116 ps). In contrast, above the cmc the NMRD profile of Gd**L** displays a hump at intermediate field, typical of slow tumbling species (Fig. 2c).[11,15,35]

The relaxivity decreases with increasing temperature, indicating that it is not limited by slow water exchange. The same behaviour was previously observed for gold nanoparticles functionalised with the analogous cysteine conjugate Gd[(DO_3A-*N*-(α-cystamido)propionate)].[15] The water exchange rate on Gd**L** is similar to that reported for the low molecular weight amide analogue Gd[(DO_3A-*N*-(α-benzoylamido)propionate)][21] and slightly higher than that reported for the parent Gd[(DO_3A-*N*-

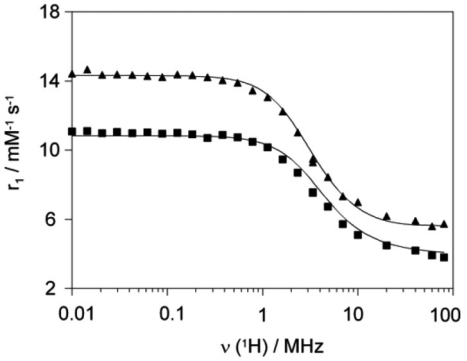

Fig. 3 ^{1}H nuclear magnetic relaxation dispersion (NMRD) profiles of Gd**L** in the monomer state at 0.3 mM at 25 °C (▲) and 37 °C (■). The curves represent results from the fittings as described in the text.

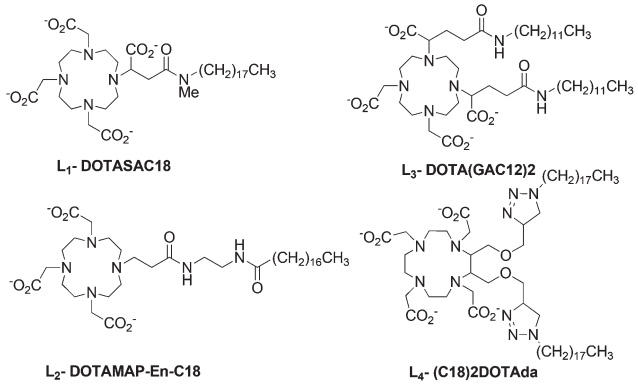

Fig. 4 Structure of amphiphilic DOTA-type ligands compared in Table 2 and discussed in the text.

(α-amino)propionate)][18] complex ($k_{ex}^{298}/10^7$ = 6.2, 5.7 and 4.0 s^{-1}, respectively). This value is in the ideal range for attaining high relaxivities at intermediate magnetic fields relevant for clinical applications.[19]

The Lipari–Szabo analysis of the longitudinal ^{1}H and ^{17}O relaxation rates allows separating fast local rotational motions of the chelate (τ_{Rl} = 930 ps) from the global rotational correlation time (τ_{Rg} = 3780 ps) of the micellar aggregate. The value of the order parameter for Gd**L** (S^2 = 0.24) is similar to those calculated for amphiphilic DOTA-type complexes functionalised with hexadecyl alkyl chains: Gd(**DOTASAC18**)[37] and Gd(**DOTAMAP-En-C18**)[38] (S^2 = 0.24 and 0.28, respectively) (Fig. 4 and Table 2).

Complexes functionalised with two long alkyl chains, Gd[(**C18)$_2$DOTAda**)][39] and Gd[(**DOTA(GAC$_{12}$)$_2$**)],[40] are characterised by substantially higher order parameters (S^2 = 0.78 and 0.70, respectively). Tighter packing of the monomers and double anchoring through adjacent sites into the micelle structure restrict internal rotational movements of the chelates.

Moreover, the complex Gd[(**C18)$_2$DOTAda**)] functionalised with two alkyl chains displays a much lower cmc value than the complex Gd(**DOTASAC18**) functionalised with one alkyl chain. In this respect, the Gd**L** complex displays a relatively high cmc value (0.6 *vs.* 0.06 and 0.004 mM for Gd[(**C18)$_2$DOTAda**)] and Gd(**DOTASAC18**), respectively) reflecting probably the aromatic nature of the pyrene lipophylic moiety and the deviation of the overall shape of the conjugate from the wedge-like geometry which would be ideal for micelle formation.

Table 2 Molecular parameters for amphiphilic DOTA-type complexes

Chelate	MW (g mol^{-1})	cmc (mM)	τ_l^{298} (ps)	τ_g^{298} (ps)	S^2	k_{ex}^{298} (/10^7 s^{-1})	r_1^{m},^{f} (mM^{-1} s^{-1})
Gd**L**$_1$[a]	881.2	0.06	330	2810	0.28	0.48	20.7
Gd**L**$_2$[b]	881.2	—	271	2696	0.21	8.12	24.2
Gd**L**$_3$[c]	1036	<0.1	820	4700	0.70	0.34	34.8
Gd**L**$_4$[d]	1285	0.004	135	5206	0.78	0.30	35
Gd**L**[e]	857	0.6	930	3780	0.24	6.2	32.2

[a] Ref. 37. [b] Ref. 38. [c] Ref. 40. [d] Ref. 39. [e] This work. [f] (20 MHz, 25 °C).

The relaxivity displayed by the micellar form of Gd**L** (32 mM^{-1} s^{-1}, 20 MHz, 25 °C) is substantially higher than that shown by the Gd(**DOTASAC18**) and Gd(**DOTAMAP-En-C18**) complexes (24.2 and 20.7 mM^{-1} s^{-1}, respectively) and it is similar to the relaxivity of the double chain chelates Gd[(**C18)$_2$DOTAda**)] and Gd[(**DOTA(GAC$_{12}$)$_2$**)] (35 and 34.8 mM^{-1} s^{-1}, respectively). The high relaxivity of the double chain chelates has been ascribed to restricted local motions of the complex (S^2 = 0.78) and to the slow global rotational motion (τ_g). Importantly, Gd**L** displays a relaxivity similar to that of the double chain chelates, despite a lower global rotational correlation time (τ_g = 3780 *vs.* 5206 and 4700 ps for Gd[(**C18)$_2$DOTAda**)] and Gd[(**DOTA(GAC$_{12}$)$_2$**)], respectively) and a substantially lower degree of coupling of global and local rotational motions (higher flexibility) (S^2 = 0.24 *vs.* 0.78 and 0.70 for Gd[(**C18)$_2$DOTAda**)] and Gd[(**DOTA(GAC$_{12}$)$_2$**)], respectively). Importantly, the relaxivity of the double chain chelates is limited by slow water exchange ($k_{ex}^{298}/10^7$ = 6.2 *vs.* 0.30 and 0.34 s^{-1} for Gd**L** and Gd[(**C18)$_2$DOTAda**)] and Gd[(**DOTA-(GAC$_{12}$)$_2$**)], respectively).

The high relaxivity attained by Gd**L** can be thus ascribed to simultaneous optimization of τ_R and k_{ex}. The optimization of the rotational dynamics of complexes has been firmly established for relaxivity enhancement at intermediate fields. The simultaneous optimization of τ_R and k_{ex} is far more demanding and often achieved at the expense of complex stability compromising potential biological applications. This study highlights the importance of simultaneous optimization of all molecular parameters in order to attain high relaxivities and provides further support for our claim that amide conjugates of the DO3A-*N*-α-aminopropionate chelator are valuable synthons for constructing high relaxivity safe CA for MRI.

Luminescence studies

The Gd[(DO$_3$A-*N*-(α-pyrenebutanamido)propionate)] complex was designed as a bimodal MRI/fluorescence probe. The pyrene fluorophore was selected to impart self-assembly

Table 3 Maximum absorption (λ_{abs}) and emission wavelengths (λ_{em}), molar extinction coefficients (ε) and fluorescence quantum yields (Φ_F) for ligand **L** and Gd**L** complex (λ_{ex} 345 nm) in non-deoxygenated water at concentrations below the cmc

λ_{abs} [b] (nm) ($\varepsilon/10^4$ M^{-1} cm^{-1})		λ_{em} (nm)		Φ_F [a,c]	
L	Gd**L**	**L**	Gd**L**	**L**	Gd**L**
344 (3.26)	344 (4.43)				
328 (2.35)	328 (3.20)				
		377	377		
314 (1.00)	314 (1.59)				
		397	398	0.22	0.17
277 (3.60)	277 (5.59)				
		417	418		
266 (2.05)	266 (3.78)				
243 (5.62)	243 (9.19)				

[a] Relative to anthracene in ethanol (Φ = 0.27). [b] Ligand and complex at 1×10^{-5} M concentration. [c] Ligand and complex at 1×10^{-6} M concentration, non-deoxygenated solutions.

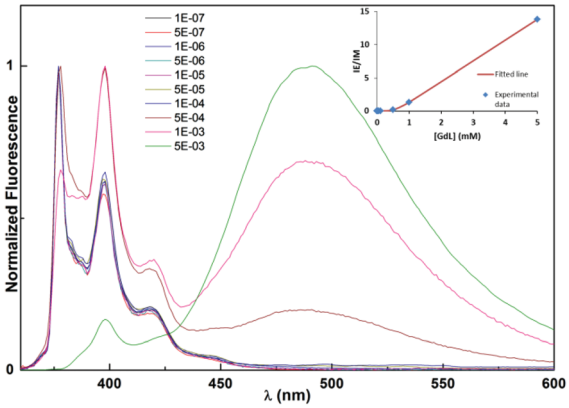

Fig. 5 Normalized fluorescence spectra for Gd**L** in non-deoxygenated water over the concentration range 1×10^{-7}–5×10^{-3} M (λ_{exc} = 345 nm). Inset – changes in the emission properties of Gd**L** as the ratio of the fluorescence emission intensity for the excimer (I_E, 490 nm) and for the monomer (I_M, 377 nm) (I_E/I_M) as a function of Gd**L** concentration.

properties and concentration-dependent fluorescence reporting capability to the paramagnetic complex.[27]

The absorption (Fig. S6†) and the fluorescence emission properties (Fig. S7†) of the free ligand **L** and the Gd**L** complex were studied in non-deoxygenated water (pH 7.0) at concentrations well below the cmc by UV-Vis and steady-state fluorescence spectroscopy (Table 3).

At concentrations below the cmc (cmc = 2.7 mM for **L**, see below, and 0.6 mM for Gd**L**), **L** and Gd**L** display similar absorption spectra in the region characteristic of pyrene (300–350 nm) assigned to intraligand π–π* transitions.[32] Selective irradiation of the pyrene chromophore on **L** and Gd**L** at 345 nm yields fluorescence spectra displaying vibronically structured features, assigned to intraligand ^{1}π–π* transitions, characteristic of pyrene monomer emission (Fig. S5†).[32,41]At the concentration studied (well below the cmc), no excimer emission (broad featureless band with an emission with an apparent maximum located at 490–500 nm) was observed for both the free ligand and the Gd^{3+} complex. The fluorescence quantum yields for **L** and for the pyrene-centred emission in Gd**L** are of the same order of magnitude as those reported for other pyrene conjugates.

Complex formation with paramagnetic Gd^{3+} seems to have only a minor effect on the fluorescence quantum yield of **L**.[41]

We envisaged that it could be possible to monitor the self-assembly process of **L** and Gd**L** by taking advantage of the aggregation-sensitive fluorescence properties of the pyrenyl moiety.[27] With this aim, we studied by steady-state fluorescence the effect of the concentration on the fluorescence properties of **L** (Fig. S7†) and Gd**L** (Fig. 5).

For low micromolar concentrations of **L** and Gd**L**, the fluorescence spectra display the characteristic vibronically structured pyrene monomer emission band. For higher (low millimolar) concentrations, the intensity of the monomer emission band is reduced and a new broad, red-shifted, featureless band, assigned to *excimer* formation, appears. The concentration dependence of the ratio of fluorescence emission intensity for the excimer (490 nm) and for the monomer (377 nm) (I_E/I_M) was used to determine independently the cmc for **L** (Fig. S7†) and Gd**L** (Fig. 5) by fitting the experimental data points to a sigmoidal curve model (Table S1†).[42,43] A cmc value of approximately 0.64 mM, in excellent agreement with the value determined by relaxometry (0.60 mM), was derived for Gd**L** from the fluorescence study (Fig. 5). A much higher cmc value (2.7 mM) was determined for the free ligand (Fig. S7†), reflecting the ionization state (multi-charged) of the free metal chelator. Below the cmc, the ligand and the complex are molecularly dissolved and the fluorescence arises from the decay of excited monomers. Above the cmc, fluorescence emission arises predominantly from the decay of excited dimers – excimers. Higher concentrations of Gd**L** increase the number of micelles and enhance excimer formation and the corresponding fluorescence emission intensity. Two different mechanisms have been established for excimer emission: diffusive encounter of an excited monomer with a ground state molecule and the direct excitation of (pre-associated) ground state dimers. The partitioning of the different modes of excimer formation depends on the fluidity of the micelle environment. Time-resolved fluorescence experiments suggest that the diffusive mechanism is the main contributor to excimer formation in cationic gemini surfactants containing a pyrene moiety and a long alkyl chain.[44] The order parameter determined for the micellar form of Gd**L** (S^2 = 0.24) indicates that the micelles are fluid, suggesting that the diffusive mechanism might be responsible for excimer formation. Deciphering the mechanism of excimer formation in Gd**L** micelles is outside the scope of the present study. The pyrene-centered fluorescence of Gd**L** effectively provides this complex with MRI/fluorescence bimodal imaging agent activity. From a practical point of view, the pyrene centred fluorescence of Gd**L** could be used for imaging studies in small

animal models, for *ex vivo* characterization of tissue distribution, cell internalization and intracellular chelate localization and studies with cell lines.[45]

Lanthanide centred fluorescence in the visible (Eu^{3+} and Tb^{3+}) and in the NIR region (Nd^{3+}, Yb^{3+}) is well suited for biological imaging for the following reasons: enhanced light penetration into biological tissues (especially in the NIR region); elimination of interference from tissue auto-fluorescence using time-gating techniques; long wavelength excitation, far into the visible region. Very low molar absorptivities (f–f transitions are forbidden by Laporte's and parity rules) make the direct excitation of Ln^{3+} ions impracticable. The formation of emissive Ln^{3+} excited states requires sensitization by sensitizing groups that absorb excitation light and transfer the resulting energy to the Ln^{3+} excited states (antenna effect), usually through ligand-centred triplet excited states.[46] In this study, we tested the possibility of using the pyrene chromophore to sensitize near infrared emitting Ln^{3+} ions in the corresponding Ln**L** complexes (Ln = Nd and Yb) (Fig. 6).

Emission spectra of the Nd**L** and Yb**L** complexes under ligand excitation exhibit metal-centred NIR emission bands at *ca.* 1064 nm ($^4F_{3/2} \rightarrow {}^4F_{13/2}$) for Nd**L** and a band with an apparent maximum at *ca.* 1000 nm ($^2F_{5/2} \rightarrow {}^2F_{7/2}$) for Yb**L**.[31,32] The excitation spectra for both luminescent Nd^{3+} and Yb^{3+} complexes are similar to each other and match well the profile of the corresponding absorption spectra as an indication that the sensitization of the lanthanide luminescence is occurring through the same electronic levels centred on pyrene.

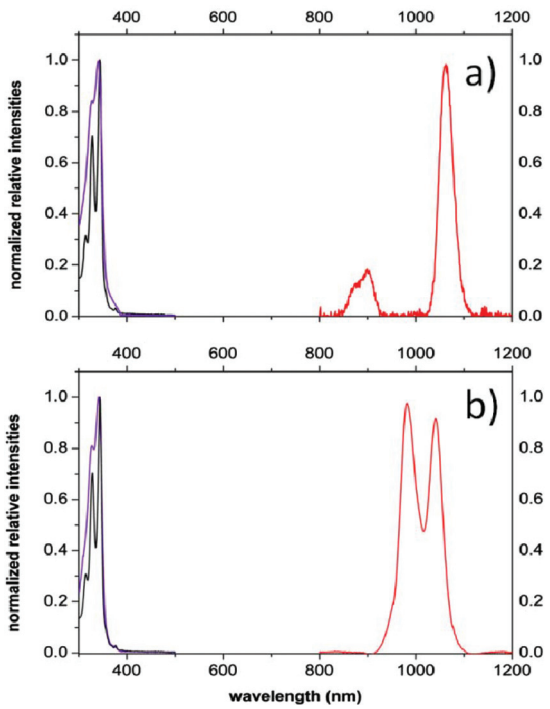

Fig. 6 Absorbance (black), excitation (λ_{em} = 1064 nm, violet) and emission (λ_{exc} = 344 nm, red) spectra for the NdL complex (a) and YbL complex (b) in water.

Interaction of GdL with human serum albumin (HSA)

Self-assembly of chelates into supramolecular structures (as discussed in this work) and binding to serum albumin (HSA) are robust strategies to enhance chelate relaxivity *via* optimization of τ_R. In addition to relaxivity enhancement, self-assembly and binding of chelates to HSA slow down CA leakage into the interstitial compartment, providing an extended time window for vasculature imaging (MRI angiography).[47] The binding affinity of Gd**L** to HSA was assessed by Proton Relaxation Enhancement (PRE) measurements. The PRE methods are tailored to determine the differences in the NMR water solvent relaxation rates between protein-bound (resulting in an increase of the relaxation rates) and free substrates. Experimentally, it consists of measuring the water proton relaxation rates R_1^{obs} in solution at increasing concentrations of the protein while keeping the concentration of the metal chelate constant (E-titration) or *vice versa* (M-titration). The data obtained for the E-titration using a Gd**L** concentration below the cmc (0.1 mM) and increasing HSA concentrations (Fig. 7) were fitted to a one site binding model (eqn (S1)†).

The fitting affords an estimation of the relaxivity of the HSA-bound form, r_1^p (53.1 ± 6.7 and 47.0 ± 5.6 mM^{-1} s^{-1} at 25 and 37 °C, respectively), and an apparent HSA-Gd**L** association constant, K_A ($K_A = 1/K_d$) ((1.9 ± 0.1) × 10^3 and (1.7 ± 0.1) × 10^3 M^{-1} at 25 and 37 °C, respectively). These values correspond to binding affinities similar to $Gd(BOPTA)^{2-}$ but weaker than those for MS-325, two blood pool agents presenting strong HSA binding.[48] Under the limiting E-titration conditions ([Gd**L**] = 0.1 mM and [HSA] = 4%), the fraction of bound chelate can be estimated as higher than 90%. These values are in line with those reported recently by Caravan for similar amide conjugates.[12] It is known that HSA has multiple binding sites. Among the many studies published on HSA binding of Gd^{3+} complexes, typically those involving ultrafiltration experiments have reported binding to more than one independent site with different binding constants.[49,50] Those stepwise binding constants show that one binding site is much stronger than the others, justifying the common use of a

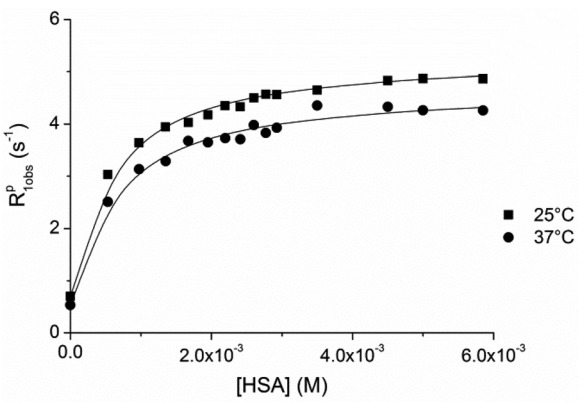

Fig. 7 Proton relaxation enhancement data (20 MHz, pH 7.4) to assess HSA binding of GdL: E-titration at 0.1 mM GdL concentration at 25 °C and 37 °C.

1 : 1 binding isotherm in interpreting the relaxometric data for albumin binding of Gd^{3+} complexes.[51] In fact, most often relaxometric data alone do not allow for distinguishing between different binding models. An independent evaluation of K_A and n may be, in principle, pursued through the analysis of the data obtained from an M-titration, in which a fixed concentration of HSA is titrated with the Gd^{3+} complex. The titration of 4% HSA with Gd**L** is restricted to the narrow range of concentrations below cmc precluding a quantitative analysis of the data. The interaction of Gd**L** with HSA is prone to modulate the biodistribution of Gd**L** as recently reported for similar conjugates.[12,52]

Biodistribution studies

The biodistribution profile of Gd**L** was obtained after 1 and 24 hours post-injection (pi) using the $^{153}Sm^{3+}$-labelled surrogate complex (Fig. 8 and Table S2†).

A recent patent claims that peptides derivatised with pyrene are able to cross the blood–brain barrier thanks to (presumably) a correct lipophylicity/hydrophylicity balance imparted by the pyrene moiety.[53] This intriguing possibility was considered during the biodistribution study. The ^{153}Sm**L** chelate displays biodistribution profiles at 1 and 24 hours pi similar to other micellar systems.[54] After 1 hour pi there is substantial activity in the blood, liver, spleen and lungs. The high activity in the blood after 1 hour pi reflects the micellar nature of the CA and its strong association with HSA, which slows down leakage of the complex into the interstitial compartment. The complex follows both hepatic and renal elimination. The hepatic and spleen uptake reflects the micellar nature of the CA and the role played by resident macrophages in the liver and spleen (Reticulo Endothelial System, RES) in clearing particulate material from the blood. The activity in the lungs might again reflect the retention of particulate material in narrow blood vessels and the extensive vascularisation of that organ and thus the high blood content of the lungs. The increase in activity in the spleen and liver after 24 hours pi correlates with the activity clearance from the blood and lungs, suggesting particle retention on those organs. Interestingly, after 1 hour pi, a low activity is measurable in the brain/cerebellum, suggesting that the complex might cross the blood–brain barrier. This possibility deserves further investigation.

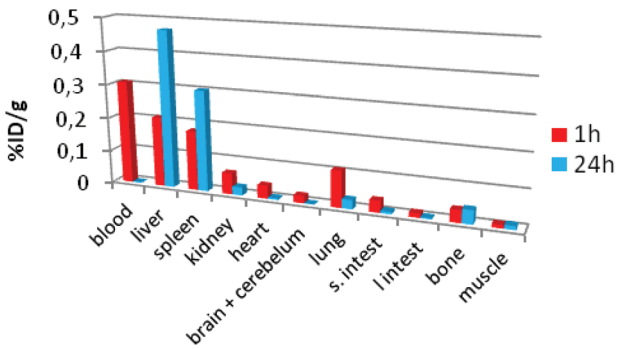

Fig. 8 Biodistribution, stated as a percentage of injected dose per gram of organ (%ID/g), of ^{153}Sm**L** in Wistar rats 1 and 24 hours after i.v. injection. Results are the mean of 4 animals.

Conclusions

The pyrenebutyric acid conjugate of the DO3A-*N*-(α-amino)propionate chelator was synthesised following synthetic methodologies reported previously by us. The lipophilic pyrene moiety imparts a concentration-dependent self-assembly ability (presumably into micelles) to the Gd[(DO_3A-*N*-(α-pyrenebutanamido)propionate)] chelate. The aggregated form of the Gd^{3+} chelate displays high relaxivity thanks to simultaneous optimization of the rotational correlation time and of the water exchange rate. Nonetheless, the relaxivity is still limited by internal flexibility. The Gd^{3+} complex displays pyrene-centred fluorescence properties sensitive to its aggregation state. The Nd^{3+} and Yb^{3+} complexes exhibit lanthanide-centred sensitized NIR emission. The surrogate $^{153}Sm^{3+}$ complex displays a biodistribution profile similar to other micellar systems. Interesting applications of this probe can be based on the recent report that carbon-based nanomaterials (graphene, graphene oxide, carbon nanotubes) functionalized non-covalently with pyrene conjugates are promising for the development of exquisite probes for biological processes.[55] In summary, we have reported recently that Gd^{3+} complexes of amide conjugates of the DO3A-*N*-(α-amino)propionate chelator are new leads for targeted, high relaxivity, safe CA for *in vivo* MRI.[21] In this work we provide further evidence to support this claim using simple design principles and robust chemistry accessible to all laboratories.

Experimental

Materials and methods

Chemicals were purchased from Sigma-Aldrich and used without further purification. Solvents used were of reagent grade and purified by usual methods. Cyclen was purchased from CheMatech, France. Reactions were monitored by TLC on Kieselgel 60 F254 (Merck) on an aluminium support. Detection was done by examination under UV light (254, 365 nm) and by adsorption of iodine vapour. Flash chromatography was performed on a Kieselgel 60 (Merck, mesh 230–400). The relevant fractions from flash chromatography were pooled and concentrated under reduced pressure, $T < 313$ K. Ion exchange chromatography was performed on Dowex 1X2-100-OH^- resin (Sigma Aldrich). The resin was purchased as the Cl^- form and converted to the OH^- form by treatment with aqueous NaOH. ^{1}H and ^{13}C NMR spectra (assigned by 2D DQF-COSY and HMQC techniques) were run on a Varian Unity Plus 300 NMR spectrometer, operating at 299.938 MHz and 75.428 MHz, for ^{1}H and ^{13}C, respectively. Chemical shifts (δ) are given in ppm relative to the $CDCl_3$ solvent (^{1}H, δ 7.27; ^{13}C, δ 77.36) as an internal standard. For ^{1}H and ^{13}C spectra recorded in D_2O, chemical shifts (δ) are given in ppm relative to TSP as the

internal reference (1H, δ 0.0) and *tert*-butanol as the external reference (^{13}C, CH_3 δ 30.29).

Synthesis of methyl 3-hydroxy-2-(4-(pyren-1-yl)butanamido)-propanoate (3). To a solution of HCl, H-Ser-OMe (**1**) (5.0 mmol, 0.778 g) and triethylamine (10 mmol) in acetonitrile (5.0 mL) were added 1-pyrenebutyric acid (**2**) (5.0 mmol, 1.44 g), 1-hidroxybenzotriazole (HOBt) (5.0 mmol, 0.675 g) and dicyclohexylcarbodiimide (DCC) (5.5 mmol, 1.13 g). The reaction mixture was left stirring at room temperature for 18 hours. The reaction mixture was filtered and the solvent was removed under reduced pressure. The residue was dissolved in ethyl acetate (100 mL), washed with $KHSO_4$ 1 M, $NaHCO_3$ 1 M and brine (3 × 30 mL each) and dried over $MgSO_4$. The solvent was removed to give **3** (1.70 g, 87%) as a yellow oil. ^{1}H NMR (300 MHz, $CDCl_3$): δ = 2.17–2.26 (m, 2H, CH_2), 2.37 (t, J = 7.2 Hz, 2H, CH_2), 3.35–3.41 (m, 2H, CH_2), 3.76 (s, 3H,CH_3), 3.86–4.00 (m, 2 H, β-CH_2 Ser), 4.66–4.71 (m, 1 H, α-CH Ser), 6.49 (d, J = 7.2 Hz, 1H, NH), 7.84 (d, J = 7.8 Hz, 1H, ArH), 7.96–8.02 (m, 3H, ArH), 8.08–8.17 (m, 4H, ArH), 8.28 (d, J = 9.3 Hz, 1H, ArH) ppm. ^{13}C NMR (75.4 MHz, $CDCl_3$): δ = 27.14 (CH_2), 32.58 (CH_2), 35.69 (CH_2), 52.72 (CH_3), 54.61 (CH), 63.40 (CH_2), 123.28 (CH), 124.74 (CH), 124.75 (CH), 124.88 (CH), 124.91 (C), 125.02 (C), 125.81 (CH), 126.68 (CH), 127.33 (CH), 127.37 (CH), 127.42 (CH), 128.70 (C), 129.91 (C), 130.82 (C), 131.24 (C), 135.61 (C), 170.93 (C═O), 173.20 (C═O) ppm. HRMS (ESI): m/z: calcd for $C_{24}H_{23}NNaO_4$, $[M + Na]^+$: 412.1520; found 412.1519.

Synthesis of methyl 2-[*N*-(*tert*-butoxycarbonyl)-4-(pyren-1-yl)-butanamido]acrylate (4). To a solution of Pyr-Ser-OMe (**3**) (5.0 mmol, 1.95 g) in dry acetonitrile (5.0 mL) were added 4-dimethylaminopyridine (DMAP) (1.7 mmmol, 0.213 g) and *tert*-butyldicarbonate (17.5 mmol, 3.82 g). The reaction mixture was left stirring at room temperature for 24 hours. The solvent was removed under reduced pressure and the residue was dissolved in ethyl acetate (100 mL). The organic layer was washed with $KHSO_4$ 1 M, $NaHCO_3$ 1 M and brine (3 × 30 mL, each), dried over $MgSO_4$ and the solvent removed under reduced pressure to give **4** (1.91 g, 81%) as a yellow oil. ^{1}H NMR (400 MHz, $CDCl_3$): δ = 1.46 (s, 9 H, CH_3 Boc), 2.23–2.27 (m, 2H, CH_2), 3.17 (t, J = 6.8 Hz, 2H, CH_2), 3.42–3.46 (m, 2H, CH_2), 3.81 (s, 3H, OCH_3), 5.67 (s, 1H, CH_2), 6.48 (s, 1H, CH_2), 7.91 (d, J = 7.6 Hz, 1H, ArH), 7.98–8.06 (m, 3H, ArH), 8.11–8.13 (m, 2H, ArH), 8.16–8.18 (m, 2H, ArH), 8.37 (d, J = 9.2 Hz, 1H, ArH) ppm. ^{13}C NMR (100.6 MHz, $CDCl_3$): δ = 26.82 (CH_2), 27.81 [C(CH_3)$_3$], 32.91 (CH_2), 37.44 (CH_2), 52.47 (OCH_3), 83.72 [O*C*(CH_3)$_3$], 123.56 (CH), 124.67 (CH), 124.77 (CH), 124.79 (CH_2), 124.99 (C), 125.06 (C), 125.74 (CH), 125.90 (CH), 126.58 (CH), 127.29 (CH), 127.34 (CH), 127.47 (CH), 128.77 (C), 129.88 (C), 130.93 (C), 131.40 (C), 135.55 (C), 136.29 (C), 151.52 (C═O), 163.68 (C═O), 175.21 (C═O) ppm. HRMS (ESI): m/z: calcd for $C_{29}H_{29}NNaO_5$, $[M + Na]^+$: 494.1943; found 494.1929.

Synthesis of (2-(*N*-*t*-butoxycarbonyl)pyrenebutyramido)-methoxycarbonylethyl-1,4,7,10-tetrazacyclododecane (monoalkylated cyclen) (6). K_2CO_3 (1.47 g, 10.6 mmol) was added to a solution of cyclen (**5**) (0.460 g, 2.67 mmol) in MeCN (30 mL). To this solution was added (pyrene)Boc-Δ-AlaOMe (**4**) (0.840 g, 1.78 mmol). The suspension was vigorously stirred at room temperature for 5 hours. The suspended solid was removed by filtration and the solvent was evaporated under reduced pressure. The residue was purified by flash chromatography (100% CH_2Cl_2 → CH_2Cl_2–EtOH–NH_4OH–H_2O (50 : 50 : 1 : 1)) to afford compound **6** as a viscous light yellow oil (0.95 g, 83%). ^{1}H NMR (300 MHz, $CDCl_3$): δ = 1.47 (s, 9H, Boc), 2.20 (m, 2H, $CH_2CH_2CH_2$), 2.50–2.80 (m, 16H, N(CH_2)$_2$N-cyclen), 3.01–3.18 (m, 2H, C(O)CH_2CH_2), 3.38–3.50 (m, 2H, CH_2CH_2-Pyrene), 2.77 (dd, J = 14.4 and 6.9 Hz, 1 H, NCH_aH$_b$CH), 3.38 (dd, J = 14.25 and 5.1 Hz, 1 H, NCH$_a$$H_b$CH), 3.70 (s, 3H, OMe), 5.51 (t, J = 6.9 and 4.8 Hz, 1H, NCH$_a$H$_b$*CH*), 7.85–8.40 (9H, m, Ar). ^{13}C NMR (75.4 MHz, $CDCl_3$): δ = 26.98 (βCH_2-Ser), 27.88 (C(*C*H$_3$)$_3$), 32.85 (γCH_2), 37.79 (αCH_2), 45.02 (CH_2), 45.37 (CH_2), 46.75 (CH_2), 51.22 (CH_2), 52.22 (OCH_3), 53.52 (CH), 55.97 (N*C*H$_2$CH), 84.31 (*C*(CH$_3$)$_3$), 123.41 (CH-Ar), 124.70 (CH-Ar), 124.72 (CH-Ar), 124.87 (CH-Ar), 125.83 (CH-Ar), 126,67 (CH-Ar), 127.37 (2 × (CH-Ar)), 127.45 (CH-Ar), 128.01 (C-Ar), 128.62 (C-Ar), 129.86 (C-Ar), 130.82 (C-Ar), 131.31 (C-Ar), 136.13 (C-Ar), 151.86 (N*C*-(O)), 170.63 (*C*(O)OCH$_3$), 175.37 (*C*(O)CH$_2$). HRMS (ESI): m/z: calcd for $C_{37}H_{50}N_5O_5$, $[M + H]^+$: 644.3812, found: 644.3807.

Synthesis of 2-pyrenebutyramido-methoxycarbonylethyl-4,7,10-tris-(ethoxycarbonylmethyl)-1,4,7,10 tetrazacyclododecane (tetraalkylated cyclen) (7). A solution of monoalkylated cyclen (**6**) (0.860 g, 1.33 mmol) in trifluoroacetic acid in dichloromethane (60%, 25 mL) was stirred overnight at room temperature. The solvent was evaporated at reduced pressure and the residue was re-dissolved in dichloromethane. This procedure was repeated several times to give a light yellow thick oil. ^{1}H NMR spectroscopy ($CDCl_3$) revealed the disappearance of the signal assigned to the *tert*-butyloxycarbonyl group in compound **6**. K_2CO_3 (2.20 g, 15.96 mmol) was added to a solution of deprotected **6** (1.33 mmol, quantitative deprotection was assumed) in MeCN (30 mL). To this suspension was added ethyl bromoacetate (0.55 mL, 4.66 mmol). The suspension was vigorously stirred at room temperature for 2.5 hours. The solid in suspension was removed by filtration, the solvent was evaporated under reduced pressure and the residue was purified by flash chromatography (100% CH_2Cl_2 → CH_2Cl_2–EtOH (1 : 1)) to afford compound **7** (0.632 g, 59%) as a white foam. ^{1}H NMR (300 MHz, $CDCl_3$): δ = 1.26 (m, 9H, 3 × CH_2CH_3), 2.20 (m, 2H, $CH_2CH_2CH_2$), 2.56 (m, 2H, C(O)CH_2CH_2), 2.60–2.90 (m, 6H, NCH_2C(O)), 2.90–3.70 (m, 16H, N(CH_2)$_2$N), 3.37 (m, 2H, CH_2CH_2 Pyrene), 3.73 (s, 3H, OMe), 3.92 (bd, 2H, NCH_2CH), 4.09 (m, 6 H, CH_2CH_3), 4.94 (bd, 1H, NCH$_2$*CH*), 7.80–8.40 (9H, m, Ar). ^{13}C NMR (75.4 MHz, $CDCl_3$): selected signals: 13.84, 13.88, 14.05 (CH_2CH_3), 27.36 (βCH_2-Ser), 32.79 (γCH_2), 35.45 (αCH_2), 48.21 (*CH*), 48.91 (CH_2), 50.34 (CH_2), 51.36 (CH_2), 52.47 (OCH_3), 53.01 (CH_2), 53.60 (*C*H$_2$CH), 54.90 (CH_2), 55.19 (CH_2), 55.71 (CH_2), 55.98 (CH_2), 58.25 (CH_2), 60.51 (CH_2), 60.99, 61.20, 61.55 (O*C*H$_2$), 123.63 (CH-Ar), 124.62 (CH-Ar), 124.75 (CH-Ar), 124.85 (CH-Ar), 125.76 (CH-Ar), 126.51 (CH-Ar), 127.18 (CH-Ar), 127.41 (CH-Ar), 127.46 (CH-Ar), 128.67 (C-Ar), 129.72 (C-Ar), 130.87 (C-Ar), 131.32 (2 × (C-Ar)), 136.43 (C-Ar), 136.53 (C-Ar), 170.312 (*C*(O)OCH$_3$), 170.53 (*C*(O)-OCH$_2$), 173.15 (*C*(O)OCH$_2$), 173.55 (*C*(O)OCH$_2$), 174.31 (NC-

(O)). HRMS (ESI): *m*/*z*: calcd for $C_{44}H_{60}N_5O_9$, $[M + H]^+$: 802.4391, found: 802.4386.

Synthesis of 2-pyrenebutyramido-carboxyethyl-4,7,10-tris-(carboxymethyl)-1,4,7,10-tetrazacyclododecane (L) (DO3A-*N*-(α-pyrenebutyramido)propionate metal chelator). Compound (7) (0.566 g, 0.710 mmol) was dissolved in a mixture made up of 20 mL of water and 20 mL of ethanol. The solution was adjusted to pH 10–11 by adding small portions of Dowex 1X2-100-OH^- resin. The suspension was kept stirring at room temperature for 2 hours. The wet resin was transferred into a chromatography column, washed with water (~50 mL) and eluted with 0.1 M hydrochloric acid, followed by a mixture of hydrochloric acid 0.1 M–ethanol (1 : 1). The relevant fractions, identified by TLC (ethanol–water 1/1, detection using iodine vapour and analysis under UV light at 365 nm), were pooled, concentrated at room temperature and further dried under vacuum to afford the final compound, as a hydrochloride, as a light yellow solid (0.31 g, 62%). ^{1}H NMR (300 MHz, D_2O/MeOD): δ = 2.13 (bb, 2H, $CH_2CH_2CH_2$), 2.50 (m, 2H, C(O)-CH_2CH_2), (2.9–3.6, broad, overlapped signals with an integration corresponding to 18H, 4 × N(CH_2)$_2$N and NCH_2CH), 3.33 (m, 2H, CH_2CH_2Pyrene), 3.81 (broad, overlapped signals with an integration corresponding to 6H, NCH_2), 4.76 (m (br), 1H, *CH*), 7.80–8.40 (9H, m, Ar). ^{13}C NMR (75.4 MHz, D_2O/MeOD): selected signals: 28.22 (βCH_2), 33.25 (γCH_2), 36.29 (αCH_2), 50.49 (bb, CH_2), 54.95 (bb, CH_2), 124.31 (CH-Ar), 125.44 (C-Ar), 125.54 (C-Ar), 125.75 (CH-Ar), 125.85 (2 × (CH-Ar)), 127.08 (CH-Ar), 127.50 (CH-Ar), 127.08 (C-Ar), 128.18 (CH-Ar), 128.37 (CH-Ar), 128.46 (CH-Ar), 129.41 (C-Ar), 130.75 (C-Ar), 131.75 (C-Ar), 137.27 (C-Ar), 177.47 (N*C*(O)). HRMS (ESI): *m*/*z*: calcd for $C_{37}H_{46}N_5O_9$, $[M + H]^+$: 704.3296, found: 704.3290.

^{1}H and ^{17}O NMR and ^{1}H NMRD experiments

Sample preparation. To an aqueous solution of the ligand (pH 5) was added drop-wise an aqueous solution of the corresponding $LnCl_3{\cdot}xH_2O$ salt in a 1 : 1 mole ratio. The solution was stirred at room temperature over 1 hour while keeping its pH at around 5.7 by adding aqueous NaOH. The solution was left stirring at room temperature overnight. Concentration under reduced pressure afforded off-white solids. Solutions for NMR measurements (20 mM) were obtained by dissolution of appropriate amounts of solid complexes in D_2O (V = 0.75 mL). Proton 1D spectra of paramagnetic (Sm^{3+} and Eu^{3+}) and diamagnetic (La^{3+}) complexes were obtained at 298 K on a Varian VNMRS 600 (14.09 T, 600.14 MHz) NMR spectrometer.

The Gd**L** complex solutions for ^{17}O NMR and ^{1}H NMRD experiments were prepared by mixing equimolar amounts of $GdCl_3$ and the ligand. A slight excess (5%) of the ligand was used. The solution was stirred at room temperature over 1 hour while keeping its pH at around 5.7 by adding aqueous NaOH. The solution was left stirring at room temperature overnight. The absence of free metal was checked by the xylenol orange test.[56,57] The pH of the stock solution was adjusted to the desired value by adding aqueous NaOH (0.1 mM). ^{17}O-enriched water (^{17}O: 11.4%) was added to the solutions for ^{17}O measurements to improve the sensitivity. The final concentration of the complex solution was 17.56 mmol kg^{-1} at pH = 6.90. For the NMRD experiments 5.0 mM and 0.1 mM solutions of the complex at pH 6.98 were used.

^{17}O NMR experiments

Variable-temperature ^{17}O NMR measurements were performed using a Bruker Avance-500 (11.7 T) spectrometer. A BVT-3000 temperature control unit was used to stabilize the temperature, measured by a substitution technique. The samples were sealed in glass spheres that fitted into 10 mm o.d. NMR tubes to eliminate susceptibility corrections to the chemical shifts.[58] Longitudinal relaxation rates ($1/T_1$) were obtained by the inversion recovery method, and transverse relaxation rates ($1/T_2$) by the Carr–Purcell–Meiboom–Gill spin-echo technique. Acidified water, pH 3.4, was used as the external reference.

NMRD measurements

The measurements were performed using a Stelar Spinmaster FFC NMR relaxometer (0.01–20 MHz) equipped with a VTC90 temperature control unit. At higher fields, the ^{1}H relaxivity measurements were performed on a Bruker electromagnet at frequencies of 30 MHz, 40 MHz, 60 MHz and 80 MHz. In each case, the temperature was measured by a substitution technique. Variable temperature measurements were performed at 25 and 37 °C.

Relaxivity studies of pH dependence and Zn^{2+} transmetallation

The transmetallation reaction of Gd**L** with Zn^{2+} was studied by following the time dependent decrease of the water proton longitudinal relaxation rate, R_1, of a phosphate-buffered saline solution (PBS, pH 7.1, 10 mM) containing 1.5 mM of Gd**L** after adding an equimolar amount of $ZnCl_2$ while the sample was vigorously stirred.[59] The water longitudinal relaxation rate was also measured as a function of time on the PBS buffered solution (pH 7.1, 10 mM) containing 2.5 mM Gd**L**.[60] The pH dependence of the relaxivity of the Gd**L** solution was studied by adjusting (pH meter) the pH of a 1 mM solution of Gd**L** in water with either NaOH or HCl solutions using a pH meter. A Bruker Minispec mq20 (20 MHz, 298 K) relaxometer was used for all measurements.

Fluorescence measurements

The absorption and the ligand-based fluorescence emission spectra of the free ligand **L** and the Gd**L** complex were recorded, respectively, using a Jasco V-630 UV-Vis spectrophotometer and a HORIBA JobinYvon Fluoromax-4 spectrofluorimeter, equipped with a monochromator in both excitation and emission and a temperature controlled cuvette holder. Fluorescence spectra were corrected for the instrumental response of the system.

The fluorescence quantum yields (Φ_s) were determined using a standard method.[61,62] Anthracene in ethanol (Φ_r = 0.27)[63] was used as the reference.

For lanthanide centred fluorescence studies in the visible (Eu^{3+} and Tb^{3+}) and in the NIR region (Nd^{3+}, Yb^{3+}), absorbance

UV spectra were performed on a Uvikon spectrophotometer, while emission and excitation (lanthanide luminescence) spectra were measured using a modified Jobin-Yvon Horiba Fluorolog-322 spectrofluorimeter equipped with a Hamamatsu R928 detector (for the visible domain) and a DSS-IGA020L (Electro-Optical Systems, Inc.) detector (for the NIR domain). Luminescence and excitation spectra were corrected for variations in lamp output, the non-linear response of the detector and the use of neutral density filters (where applicable). For collecting luminescence data, samples were placed in quartz Suprasil cells (Hellma® 115F-QS, bandpass 0.2 cm).

Biodistribution studies

^{153}Sm**L** for *in vivo* experiments was prepared by adding 1 mCi of [^{153}Sm]Cl_3 (produced at the Instituto Tecnológico e Nuclear, Lisbon, Portugal with a specific radioactivity >5 GBq mg^{-1}) to a solution of 1 mg of the chelator in acetate buffer (400 μL, 0.4 M, pH 5) and heated at 80 °C for *ca*. 1 hour. The radiochemical purity of ^{153}Sm$\mathbf{L_1}$ was determined by TLC. The percentage of chelated metal was found to be greater than 95%.

Groups of four animals (Wistar male rats weighing *ca*. 200 g) were anaesthetized with ketamine (50.0 mg mL^{-1})/chloropromazine (2.5%) (10 : 3) and injected in the tail vein with *ca*. 100 μCi of the tracer. Animals were sacrificed 1 and 24 hours later and the major organs were removed, weighed and counted in a γ well-counter.

Size distribution

The size distribution of particles in a (micellar) solution of Gd**L** at a concentration well above the cmc (5.0 mM, pH 7.0) was determined with a Malvern Zetasizer, NANO ZS (Malvern Instruments Limited, UK) using an He–Ne laser (λ = 633 nm) and a detector angle of 173°. The Gd**L** solution in a polystyrene cell (1 mL) was analysed at 25 °C. The mean hydrodynamic radius (*z*-average) and a width parameter for the distribution, polydispersity or polydispersity index (PdI) were calculated from the intensity of the scattered light. In the present work, the intensity-based *z*-average parameter was considered the best approach to the actual particle size.

Data analysis

Data obtained from ^{17}O NMR, ^{1}H NMRD, Luminescence and Quantum Yield measurement studies were processed using OriginLab Pro 8 SRO. Data from relaxometric and transmetallation studies were processed using Microsoft Office Excel 2007.

Acknowledgements

This work was financially supported by Fundação para a Ciência e Tecnologia, Portugal: project PTDC/QUI/70063/2006, including a grant to C.I.O.M., grant SFRH/BD/63994/2009 to M.F.F., grant SFRH/BD/46370/2008 to A.F.M. and sabbatical grant SFRH/BSAB/ 1328/2013 to J.A.M. and Rede Nacional de RMN (REDE/1517/RMN/2005) for the acquisition of the Varian VNMRS 600 NMR spectrometer in Coimbra. The work in France was supported by La Ligue contre le Cancer. This work was carried out in the framework of the COST Actions D38 "Metal Based Systems for Molecular Imaging", TD1004 "Theragnostic Imaging" and CM1006 "EUFEN: European F-Element Network". S.P. acknowledges support from the Institut National de la Santé et de la Recherche Médicale (INSERM).

References

1 M. L. James and S. S. Gambhir, *Physiol. Rev.*, 2012, **92**, 897.
2 P. Caravan, J. J. Ellison, T. J. McMurry and R. B. Lauffer, *Chem. Rev.*, 1999, **99**, 2293.
3 *The Chemistry of Contrast Agents in Medical Magnetic Resonance Imaging*, ed. A. Merbach, L. Helm and É. Tóth, Wiley, Chichester, 2nd edn, 2013.
4 L. Helm, *Prog. Nucl. Magn. Reson. Spectrosc.*, 2006, **49**, 45.
5 P. Marckmann, L. Skov, K. Rossen, A. Dupont, M. B. Damholt, J. G. Heaf and H. S. Thomsen, *J. Am. Soc. Nephrol.*, 2006, **17**, 2359.
6 J. C. Weinreb and A. K. Abu-Alfa, *J. Magn. Reson. Imaging*, 2009, **30**, 1236.
7 M. Port, J.-M. Idée, C. Medina, C. Robic, M. Sabatou and C. Corot, *BioMetals*, 2008, **21**, 469.
8 S. K. Morcos, *Eur. J. Radiol.*, 2008, **66**, 175.
9 P. Caravan, C. T. Farrar, L. Frullano and R. Uppal, *Contrast Media Mol. Imaging*, 2009, **4**, 89.
10 A. Borel, J. F. Bean, R. B. Clarkson, L. Helm, L. Moriggi, A. D. Sherry and M. Woods, *Chem.–Eur. J.*, 2008, **14**, 2658.
11 S. Torres, J. A. Martins, J. P. André, C. F. G. C. Geraldes, A. E. Merbach and E. Tóth, *Chem.–Eur. J.*, 2006, **12**, 940.
12 E. Boros and P. Caravan, *J. Med. Chem.*, 2013, **56**, 1782.
13 Z. Zhang, M. T. Greenfield, M. Spiller, T. J. McMurry, R. B. Lauffer and P. Caravan, *Angew. Chem., Int. Ed.*, 2005, **44**, 6766.
14 É. Tóth, D. Pubanz, S. Vauthey, L. Helm and A. E. Merbach, *Chem.–Eur. J.*, 1996, **2**, 1607.
15 M. F. Ferreira, B. Mousavi, P. M. Ferreira, C. I. O. Martins, L. Helm, J. A. Martins and C. F. G. C. Geraldes, *Dalton Trans.*, 2012, **41**, 5472.
16 S. Qazi, L. O. Liepold, M. J. Abedin, B. Johnson, P. Prevelige, J. A. Frank and T. Douglas, *Mol. Pharmaceutics*, 2013, **10**, 11.
17 G. J. Stasiuk, S. Tamang, D. Imbert, C. Poillot, M. Giardiello, C. Tisseyre, E. L. Barbier, P. H. Fries, M. de Waard, P. Reiss and M. Mazzanti, *ACS Nano*, 2011, **5**, 8193.
18 M. F. Ferreira, A. F. Martins, J. A. Martins, P. M. Ferreira, E. Toth and C. F. G. C. Geraldes, *Chem. Commun.*, 2009, 6475.
19 Z. Jaszberenyi, A. Sour, É. Tóth, M. Benmelouka and A. E. Merbach, *Dalton Trans.*, 2005, 2713.
20 E. Balogh, R. Tripier, P. Fouskova, F. Reviriego, H. Handel and É. Tóth, *Dalton Trans.*, 2007, 3572.
21 M. F. Ferreira, A. F. Martins, C. I. O. Martins, P. M. Ferreira, É. Tóth, T. B. Rodrigues, D. Calle, S. Cerdan, P. Lopez-

Larrubia, J. A. Martins and C. F. G. C. Geraldes, *Contrast Media Mol. Imaging*, 2013, **8**, 40.
22 A. Louie, *Chem. Rev.*, 2010, **110**, 3146.
23 Y. Song, H. Zong, E. R. Trivedi, B. J. Vesper, E. A. Waters, A. G. M. Barrett, J. A. Radosevich, B. M. Hoffman and T. J. Meade, *Bioconjugate Chem.*, 2010, **21**, 2267.
24 W. J. M. Mulder, R. Koole, R. J. Brandwijk, G. Storm, P. T. K. Chin, G. J. Strijkers, C. M. Donega, K. Nicolay and A. W. Griffioen, *Nano Lett.*, 2006, **6**, 2.
25 S. L. C. Pinho, H. Faneca, C. F. G. C. Geraldes, M.-H. Delville, L. D. Carlos and J. Rocha, *Biomaterials*, 2012, **33**, 925.
26 E. Lipani, S. Laurent, M. Surin, L. Vander Elst, P. Leclère and R. N. Muller, *Langmuir*, 2013, **29**, 3419.
27 F. M. Winnik, *Chem. Rev.*, 1993, **93**, 587.
28 J. Duhamel, *Langmuir*, 2012, **28**, 6527.
29 Z. Wang, P. Huang, A. Bhirde, A. Jin, Y. Ma, G. Niu, N. Neamati and X. Chen, *Chem. Commun.*, 2012, **48**, 9768.
30 S. Karuppannan and J.-C. Chambron, *Chem.–Asian J.*, 2011, **6**, 964.
31 S. Faulkner, M.-C. Carrié, S. J. A. Pope, J. Squire, A. Beeby and P. G. Sammes, *Dalton Trans.*, 2004, 1405.
32 S. J. A. Pope, *Polyhedron*, 2007, **26**, 4818.
33 P. M. T. Ferreira and H. L. S. Maia, *J. Chem. Soc., Perkin Trans.*, 1999, **1**, 3697.
34 E. Boros, M. Polasek, Z. Zhang and P. Caravan, *J. Am. Chem. Soc.*, 2012, **134**, 19858.
35 F. A. Dunand, E. Tóth, R. Hollister and A. E. Merbach, *J. Biol. Inorg. Chem.*, 2001, **6**, 247.
36 D. H. Powell, O. M. N. Dhubhghaill, D. Pubanz, L. Helm, Y. S. Lebedev, W. Schlaepfer and A. E. Merbach, *J. Am. Chem. Soc.*, 1996, **118**, 9333.
37 J. P. André, E. Tóth, H. Fischer, A. Seelig, H. R. Mäcke and A. E. Merbach, *Chem.–Eur. J.*, 1999, **5**, 2977.
38 L. Tei, G. Gugliotta, Z. Baranyai and M. Botta, *Dalton Trans.*, 2009, 9712.
39 C. Vanasschen, N. Bouslimani, D. Thonon and J. F. Desreux, *Inorg. Chem.*, 2011, **50**, 8946.
40 F. Kielar, L. Tei, E. Terreno and M. Botta, *J. Am. Chem. Soc.*, 2010, **132**, 7836.
41 J. P. Holland, V. Fisher, J. A. Hickin and J. M. Peach, *Eur. J. Inorg. Chem.*, 2010, 48.
42 C. Wang, S. D. Wettig, M. Foldvari and R. E. Verrall, *Langmuir*, 2007, **23**, 8995.
43 P. Carpena, J. Aguiar, P. Bernaola-Galván and C. Carnero Ruiz, *Langmuir*, 2002, **18**, 6054.
44 C. Keyes-Baig, J. Duhamel and S. Wettig, *Langmuir*, 2011, **27**, 3361.
45 K. Lim, A. Price, S.-F. Chong, B. M. Paterson, A. Caragounis, K. J. Barnham, P. J. Crouch, J. M. Peach, J. R. Dilworth, A. R. White and P. S. Donnelly, *J. Biol. Inorg. Chem.*, 2010, **15**, 225.
46 J.-C. G. Bunzli, *Chem. Rev.*, 2010, **110**, 2729.
47 R. B. Lauffer, D. J. Parmelee, S. U. Dunham, H. S. Quellet, R. P. Dolan, S. White, T. J. McMurry and R. C. Walovitch, *Radiology*, 1988, **207**, 529.
48 V. Henrotte, L. Vander Elst, S. Laurent and R. N. Muller, *J. Biol. Inorg. Chem.*, 2007, **12**, 929.
49 P. Caravan, N. J. Cloutier, M. T. Greenfield, S. A. McDermid, S. U. Dunham, J. W. M. Bulte, J. C. Amedio Jr., R. J. Looby, R. M. Supkowski, R. M. Horrocks Jr., T. J. McMurry and R. B. Lauffer, *J. Am. Chem. Soc.*, 2002, **124**, 3152.
50 L. Moriggi, M. A. Yaseen, L. Helm and P. Caravan, *Chem. Weinh. Bergstr. Ger.*, 2012, **18**, 3675.
51 M. Giardiello, M. Botta and M. P. Lowe, *J. Inclusion Phenom. Macrocyclic Chem.*, 2011, **71**, 435.
52 A. F. Martins, J.-F. Morfin, A. Kubíčková, V. Kubíček, F. Buron, F. Suzenet, M. Salerno, A. N. Lazar, C. Duyckaerts, N. Arlicot, D. Guilloteau, C. F. G. C. Geraldes and É. Tóth, *ACS Med. Chem. Lett.*, 2013, **5**, 436.
53 R. Wegrzyn, A. Nyborg, D. R. Duan and A. Rudolf, *Patent WO*, 2009117041 A2, 2009.
54 S. Torres, M. I. M. Prata, A. C. Santos, J. P. André, J. A. Martins, L. Helm, E. Tóth, M. L. García-Martín, T. B. Rodrigues, P. López-Larrubia, S. Cerdán and C. F. G. C. Geraldes, *NMR Biomed.*, 2008, **21**, 322.
55 K. Furukawa, Y. Ueno, E. Tamechika and H. i. Hibino, *J. Mater. Chem. B*, 2013, **1**, 1119.
56 R. Hovland, A. J. Aasen and J. Klaveness, *Org. Biomol. Chem.*, 2003, **1**, 1707.
57 A. Barge, G. Cravotto, E. Gianolio and F. Fedeli, *Contrast Media Mol. Imaging*, 2006, **1**, 184.
58 A. D. Hugi, L. Helm and A. E. Merbach, *Inorg. Chem.*, 1987, **26**, 1763.
59 S. Laurent, L. V. Elst, F. Copoix and R. N. Muller, *Invest. Radiol.*, 2001, **36**, 115.
60 S. Laurent, L. V. Elst, A. Vroman and R. N. Muller, *Helv. Chim. Acta*, 2007, **90**, 562.
61 J. N. Demas and G. A. Crosby, *J. Phys. Chem.*, 1971, **75**, 991.
62 S. Fery-Forgues and D. Lavabre, *J. Chem. Educ.*, 1999, **76**, 1260.
63 J. V. Morris, M. A. Mahaney and J. R. Huber, *J. Phys. Chem.*, 1976, **80**, 969.